

RESEARCH ARTICLE

# The three dimensional structure of Bovine Salivary Protein 30b (BSP30b) and its interaction with specific rumen bacteria

Heng Zhang<sup>1</sup>, Judith Burrows<sup>1</sup>, Graeme L. Card<sup>2\*</sup>, Graeme Attwood<sup>3</sup>, Tom T. Wheeler<sup>4</sup>, Vickery L. Arcus<sup>1\*</sup>

**1** School of Science, University of Waikato, Hamilton, New Zealand, **2** Stanford Synchrotron Radiation Lightsource, Menlo Park, California, United States of America, **3** AgResearch Grasslands, Tennent Drive, Palmerston North, New Zealand, **4** Cawthron Research Institute, The Wood, Nelson, New Zealand

✉ Current address: 35 Prisk Street, Melville, Hamilton, New Zealand

\* [varcus@waikato.ac.nz](mailto:varcus@waikato.ac.nz)



**OPEN ACCESS**

**Citation:** Zhang H, Burrows J, Card GL, Attwood G, Wheeler TT, Arcus VL (2019) The three dimensional structure of Bovine Salivary Protein 30b (BSP30b) and its interaction with specific rumen bacteria. PLoS ONE 14(4): e0206709. <https://doi.org/10.1371/journal.pone.0206709>

**Editor:** Travis Beddoe, La Trobe University, AUSTRALIA

**Received:** October 15, 2018

**Accepted:** March 26, 2019

**Published:** April 12, 2019

**Copyright:** © 2019 Zhang et al. This is an open access article distributed under the terms of the [Creative Commons Attribution License](https://creativecommons.org/licenses/by/4.0/), which permits unrestricted use, distribution, and reproduction in any medium, provided the original author and source are credited.

**Data Availability Statement:** The diffraction data and structure files for BSP30b has been deposited at the Protein Data Bank with accession codes 5WD6 & 601T.

**Funding:** This work was supported by Dairy NZ (<https://www.dairynz.co.nz/>) to HZ. The funder had no role in study design, data collection and analysis, decision to publish, or preparation of the manuscript.

**Competing interests:** The authors have declared that no competing interests exist.

## Abstract

Bovine Salivary Protein 30b (BSP30b) is a member of the tubular lipid-binding (TULIP) superfamily that includes the human bactericidal/permeability-increasing proteins (BPI), lipopolysaccharide binding proteins (LBP) and palate, lung, and nasal epithelium carcinoma-associated proteins (PLUNC). BSP30b is most closely related to the PLUNC family and is predominantly found in bovine saliva. There are four BSP30 isoforms (BSP30a-d) and collectively, they are the most abundant protein component of bovine saliva. The PLUNC family members are proposed to be lipid binding proteins, although in most cases their lipid ligands are unknown. Here, we present the X-ray crystal structure of BSP30b at 2.0 Å resolution. We used a double methionine mutant and Se-Met SAD phasing to solve the structure. The structure adopts a curved cylindrical form with a hydrophobic channel formed by an  $\alpha/\beta$  wrap, which is consistent with the TULIP superfamily. The structure of BSP30b in complex with oleic acid is also presented where the ligand is accommodated within the hydrophobic channel. The electron density for oleic acid suggests that the ligand is only partially occupied in the binding site implying that oleic acid may not be the preferred ligand. GFP-tagged BSP30b binds to the surface of olive oil droplets, as observed under fluorescent microscopy, and acts as a surfactant consistent with its association with decreased susceptibility to bloat in cattle. Bacteria extracted directly from bovine rumen contents indicate that the GFP\_BSP30b fusion protein binds to a small number of selected bacterial species *in vivo*. These results suggest that BSP30b may bind to bacterial lipids from specific species and that this abundant protein may have important biological roles via interacting with rumen bacteria during feeding and rumination.

## Introduction

PLUNC (palate, lung, and nasal epithelium carcinoma-associated) proteins are a family of proteins predominantly expressed in the upper respiratory tract, nasal mucosa, and oral cavity in

**Abbreviations:** BPI, bactericidal/permeability-increasing; BSP30b, bovine salivary protein 30b; PLUNC, palate, lung, and nasal epithelium carcinoma-associated; TULIP, tubular lipid-binding.

mammals. PLUNC proteins are further subdivided into LPLUNC (long PLUNC) proteins and SPLUNC (short PLUNC) proteins [1]. Although several studies have characterized the expression of PLUNC proteins, their biological function(s) are not well understood. Studies have reported that PLUNCs can bind to bacteria and LPS (lipopolysaccharide) [2–4] but in antimicrobial assays PLUNCs showed no bactericidal activity against *Escherichia coli* DH5-a, *P. aeruginosa* PA01 or *Listeria monocytogenes* [5].

From a structural point of view, the PLUNC protein family belongs to the TULIP (tubular lipid-binding) superfamily [6]. The tertiary structure of this domain is a long, bent helix wrapped in four highly curved anti-parallel  $\beta$ -strands, forming a central hydrophobic channel ideal for lipid binding [7]. The TULIP superfamily consists of three protein families—BPI-like, SMP-like (synaptotagmin-like, mitochondrial and lipid-binding protein), and Takeout-like protein families. The BPI-like family includes BPI, LBP, CETP (the cholesteryl ester transfer protein), PLTP (the phospholipid transfer protein), and PLUNC. These proteins are either involved in innate immunity against bacteria through their ability to bind LPS, or in lipid exchange between lipoprotein particles. The Takeout-like protein family consists of various arthropod allergens and insect juvenile hormone-binding proteins, which transport lipid hormones to target tissues during insect development. The SMP-like protein family includes subunits of the ERMES complex (ER-mitochondria encounter structures) and the extended synaptotagmins (E-Syts), which appear to be mainly located at membrane contact sites between organelles, mediating inter-organelle lipid exchange [7].

The first described PLUNC protein in cattle was named Bovine Salivary Protein 30 (BSP30), based on its mass of approximately 30 kDa [8]. This “BSP30” protein is one of the most abundant proteins in bovine saliva, with a concentration of 0.1–0.5 mg.ml<sup>-1</sup>. Its abundance was proposed to be associated with the susceptibility of cattle to pasture bloat, a metabolic disease characterized by build-up of stable foam in the rumen and hence impairment of the eructation mechanism, causing rumen distension and respiratory distress [9]. Although BSP30b has been systematically renamed as BPIFA2B in 2011 [10], in this paper, BSP30b is used for the sake of simplicity and to keep consistent with previous publications regarding this protein. Further investigation of BSP30 revealed that it is a mixture of two closely related proteins—BSP30a and BSP30b, sharing 83% amino acid identity, with expression restricted to salivary tissue [11]. Sequencing analysis of the PLUNC gene locus within cattle revealed that there are thirteen genes within this locus, nine of which are orthologous to genes in the human and mouse PLUNC gene locus [12]. The other four genes, namely *BSP30a*, *BSP30b*, *BSP30c*, and *BSP30d*, are thought to have arisen through gene duplications and are a characteristic feature of ruminants. The implication is that these proteins contribute to ruminant-specific physiological functions [12, 13]. A gene expression study indicated that the mRNAs of these four *BSP30* genes are most abundant in tissues associated with the oral cavity and airways. Notably, *BSP30a* and *BSP30b* are abundantly expressed in the salivary gland independently of one another and the proteins are secreted into saliva, accounting for 15–30% of the total protein in bovine saliva [14].

Analyses of the cattle PLUNC family at the protein level have focused on BSP30a and BSP30b. Immunohistochemical analysis of bovine salivary glands with antibodies specific for both BSP30a and BSP30b suggested that they are localized to the serous secretory cells [15]. Further analysis with Western blotting revealed that BSP30b is present in the parotid, submandibular and buccal salivary glands; whilst BSP30a is only present in the submandibular gland, although its mRNA was shown to be expressed abundantly in the parotid [13, 14]. Functional studies suggests that both BSP30a and BSP30b can suppress the growth of *Pseudomonas aeruginosa* with moderate potency but suppression was not observed for other pathogens tested,

indicating that the BSP30 proteins may not have a primary function as bactericidal proteins [13, 15]. It has also been observed that both BSP30a and BSP30b have no significant LPS binding activity, suggesting the mechanism of their moderate antibacterial activity is independent of LPS opsonisation [13].

To address functional questions regarding BSP30 proteins, we have solved the X-ray crystal structure of BSP30b at 2.0 Å resolution. The structure shows the conserved architecture seen among the TULIP superfamily. We have also solved the structure of BSP30b in complex with oleic acid which shows that the hydrophobic channel can sequester one molecule after co-crystallization. However, the electron density of oleic acid is relatively weak, suggesting it is not the preferred lipid ligand of BSP30b. We demonstrate that olive oil can be dispersed into nanodroplets after mixing with BSP30b and thus corroborate its surfactant properties. We further report that BSP30b binds to the surface of a small subset of rumen bacterial species and thus, BSP30b may bind to a specific range of lipid ligands and play a biological role in the rumen via interaction with specific rumen bacteria.

## Materials and methods

### Protein expression, crystallization, and structure determination

The double mutant Bovine BSP30b gene containing two methionine residues (replacing phenylalanine residues, *BSP30b\_F61M\_F115M*) was synthesized with restriction sites BamHI and XhoI by GeneArt (Life Technologies, Carlsbad CA). This gene was ligated into the BamHI/XhoI site of the *pProEx Htb* vector and transformed into *Escherichia coli BL21* cells. Seleno-methionine (SeMet) incorporated BSP30b\_F61M\_F115M was expressed in M9 minimal media. A cell culture was grown at 37 °C with 100 µg.mL<sup>-1</sup> ampicillin with shaking at 200 rpm. When the OD<sub>600</sub> of the culture reached 0.4–0.6, 100 mg of lysine, phenylalanine and threonine, 50 mg of isoleucine and valine, and 60 mg of selenomethionine were added and the growth was continued for a further 15 min. IPTG (0.5 mM final concentration) was added for induction of protein expression and the culture was grown overnight. Cells were harvested by centrifugation at 6000 rpm for 20 min and resuspended in 20 ml of lysis buffer (20 mM HEPES pH 8, 150 mM NaCl, 1 mM β-mercaptoethanol, 20 mM imidazole) and then sonicated on ice. Disrupted cells were centrifuged at 13,000 rpm and the soluble fraction containing BSP30b\_F61M\_F115M SeMet was loaded onto a HiTrap Ni column for protein purification. Protein was further purified with anion exchange chromatography using MONO Q 4.6/100 PE (GE Healthcare). The protein was finally purified with size exclusion chromatography (SEC) using a Superdex 75 16/60 column (GE Healthcare) and eluted with 10 mM HEPES pH 8, 150 mM NaCl. The purified protein was concentrated to 8 mg.mL<sup>-1</sup> for crystallization.

The BSP30b\_F61M\_F115M SeMet derivative was crystallized using hanging drop vapour diffusion at 18 °C by mixing 1.5 µL of the protein solution with 1.5 µL of the reservoir solution (0.1 M HEPES pH 7.5, 0.2 M CaCl<sub>2</sub>, 9% PEG 3350, and 5% isopropyl alcohol). Crystals were obtained after two weeks and were flash frozen in liquid nitrogen without cryo-protectant for data collection. Single-wavelength anomalous dispersion (SAD) data were collected using X-rays at a wavelength of 0.9537 Å at the Australian Synchrotron MX2 beamline with an ADSC Quantum 210r detector. Data were integrated using iMosflm [16] and scaled using Aimless [17] within the CCP4 platform suite 6.4.0 [18]. Phases were solved by using AutoSol [19] and the initial structure was built using AutoBuild [20] within the PHENIX platform suite [21]. The structure was first refined using *phenix.refine* [22] in PHENIX. Subsequent cycles of manual refinement using COOT 7.0 [23] and automatic refinement in PHENIX were performed.

### Co-crystallization of BSP30b\_F61M\_F115M with oleic acid

To obtain crystals of a BSP30b\_F61M\_F115M-oleic acid complex, purified protein was concentrated to  $\sim 2 \text{ mg.mL}^{-1}$  and incubated with 20  $\mu\text{L}$  of oleic acid ( $\geq 99\%$ , Sigma-Aldrich) at 4 °C overnight. This mixture was purified using SEC to remove unbound oleic acid and then concentrated to  $8 \text{ mg.mL}^{-1}$  for crystallization. Crystals were obtained after two weeks under the same conditions as for the protein alone. A complete diffraction dataset was collected at the Australian Synchrotron MX2 beamline using the new ACRF Eiger 16M detector [24]. The structure was solved by molecular replacement using Phaser [25] with the solved BSP30b structure as the reference model. The structure was built and refined as above. A polder OMIT map was calculated using *phenix.polder* in the PHENIX software package [26].

### Fluorescent microscopy of GFP\_BSP30b mixed with olive oil

A GFP\_BSP30b fusion protein was constructed to visualize the interaction between wild type BSP30b and olive oil, as well as the interaction with microorganisms in the rumen. Both GFP and wild type BSP30b were cloned into *pProEx Htb* with the BamHI/PstI and XhoI/HindIII restriction sites, respectively. GFP itself was cloned into *pProEx Htb* with the BamHI/PstI restriction sites, which was used as a control. The fused protein and GFP alone were separately expressed in LB media with a 6 x histidine tag at the N-terminus.

Since the primary lipid source for cattle is long chain fatty acids in triglyceride form, the interaction between BSP30b and triglyceride was studied to illustrate the function of BSP30b. Olive oil was chosen for this purpose as it is composed mainly of the mixed triglyceride esters of oleic acid, linoleic acid, palmitic acid and other fatty acids, similar to the composition of triglycerides from pasture grass.

20  $\mu\text{L}$  of olive oil was added to 500  $\mu\text{L}$  of GFP\_BSP30b at a concentration of  $2 \text{ mg.mL}^{-1}$ , which was then vortexed for 2 mins and left on the lab bench for 20 mins for equilibration. 10  $\mu\text{L}$  of this mixture was pipetted onto a glass slide and then covered with a cover slip. The slide was viewed by using a ZEISS AXIOSTAR (LLC, US) bench top microscope. Images were captured at 40 X magnification with filter 1 (blue light) using a Nikon Coolpix 4500 camera (Tokyo, Japan). The control experiment was performed by adding 20  $\mu\text{L}$  of olive oil to 500  $\mu\text{L}$  of GFP at a concentration of  $2 \text{ mg.mL}^{-1}$ . The same procedure was carried out for the control experiment as for GFP\_BSP30b. Images were captured at 40 X magnification under both bright field and UV illumination.

### Fluorescent microscopy of GFP\_BSP30b with rumen samples

Ethics approval for cattle rumen contents sampling: Grasslands Animal Ethics Committee Approval No. 13398 (cattle). Rumen fluid was collected from a fistulated cow at AgResearch (Palmerston North, New Zealand). After filtration through cheesecloth to remove large feed particles, the fluid was incubated at 39 °C in a waterbath and kept anaerobic by bubbling with a slow stream of  $\text{CO}_2$ . This filtered fluid was further separated into bacterial and protozoal fractions by low speed centrifugation at  $300 \times g$  for 5 min. The pellet, which contained the protozoa and some bacteria, was diluted with Artificial Saliva (142 mM  $\text{Na}_2\text{HPO}_4$ , 84 mM  $\text{NaHCO}_3$ , 100.1 mM  $\text{KHCO}_3$ , 60.1 mM Urea, and 58.4 mM NaCl) to the same volume as the supernatant. The supernatant, which then contained the bulk of the bacteria, was centrifuged at  $15,000 \times g$  for 15 min to pellet the bacteria. The bacterial pellet was then re-suspended with Artificial Saliva to the same volume as the supernatant. GFP\_BSP30b protein ( $0.1 \text{ mg.mL}^{-1}$ ) was then mixed with the protozoal or bacterial fractions at a ratio of 1:1 by volume. 20  $\mu\text{L}$  of each mixture was pipetted on a slide, covered with a coverslip and viewed under ultraviolet (UV) illumination using a Leica Model DN 2500 microscope at 100x magnification under oil.

## Results

### Structure determination and description

Crystals of a double Phe-to-Met mutant of BSP30b diffracted to 2.0 Å resolution with a space group of C2 and unit cell dimensions: a = 81.65 Å, b = 59.57 Å, c = 89.94 Å,  $\alpha = \gamma = 90^\circ$ ,  $\beta = 106.25^\circ$  (Table 1). The structure was solved using SeMet incorporated protein and SAD methods.

BSP30b crystallized with two molecules in the asymmetric unit. Each molecule consists of 7  $\alpha$  helices and 6  $\beta$  strands as well as connecting turns and loops, which constitute the conserved TULIP fold (Fig 1A). The N-terminus of the structure of BSP30b contains four consecutive helices ( $\alpha$ 1, residues 40–48;  $\alpha$ 2, residues 50–53;  $\alpha$ 3, residues 55–69;  $\alpha$ 4 residues 81–100) with the fourth helix lying antiparallel to the preceding three (Fig 1B). Electron density for the loop joining  $\alpha$ 3 and  $\alpha$ 4 is absent. This central section of the structure comprises a highly twisted 4-stranded antiparallel  $\beta$  sheet where the first and fourth strands are interrupted by a loop and a short helix respectively (Fig 1B). A long curved  $\alpha$  helix ( $\alpha$ 6 residues 193–224) follows the central section and the structure terminates with a C-terminal helix unique to the BSP30 subfamily ( $\alpha$ 7 residues 227–235).

The hydrophobic channel of BSP30b (~22.6 Å in length) is enclosed by all of the secondary structure elements. The internal cavity has a volume of 90.2 Å<sup>3</sup> as calculated by the CASTp 3.0 online server [27] and the cavity is lined by predominantly aliphatic hydrophobic residues. This internal cavity has an opening located adjacent to the C-terminal helix ( $\alpha$ 7, Fig 1A) at one end of the long axis of the structure. The flexible loop between helices  $\alpha$ 3 and  $\alpha$ 4 at the opening of the channel potentially caps the channel and may play a role in ligand binding. BSP30b also has a conserved disulfide bridge common to the PLUNC family (cysteines 172 and 225) that

Table 1. Crystallographic data collection and refinement statistics.

	BSP30b_F61M_F115M	BSP30b_F61M_F115M-oleic acid
<b>Data collection</b>		
Wavelength	0.9537 Å	0.95369 Å
Space group	C121	C121
Cell constants a, b, c, $\alpha$ , $\beta$ , $\gamma$	81.65Å 59.57Å 89.94Å 90.00° 106.25° 90.00°	83.75Å 61.40Å 91.09Å 90.00° 107.74° 90.00°
Resolution (Å)	47.43–2.00 (2.11–2.00)	86.76–2.30 (2.38–2.30)
$R_{merge}$	0.100 (0.622)	0.060 (0.222)
$R_{pim}$	0.040 (0.245)	0.039 (0.159)
CC1/2	0.998 (0.922)	0.997 (0.985)
Completeness (%)	99.9 (100)	99.8 (99.6)
Redundancy	7.2 (7.3)	5.7 (5.3)
No. of observations	201779 (29708)	112987 (10375)
No. of unique reflections	28136 (4080)	19718 (1940)
Mean I/ $\sigma$ (I)	11.8 (3.5)	15.0 (5.4)
Anomalous completeness (%)	98.5 (98.1)	
Anomalous multiplicity	3.7(3.8)	
<b>Refinement</b>		
$R_{work}$	0.205	0.223
$R_{free}$	0.251	0.265
Average B, all atoms (ligand) (Å <sup>2</sup> )	36.0	60.68 (72.79)
Ramachandran favoured (outliers)	97.05% (0.00%)	95.92% (0.54%)
Rotamer outliers	0.00%	0.00%

<https://doi.org/10.1371/journal.pone.0206709.t001>

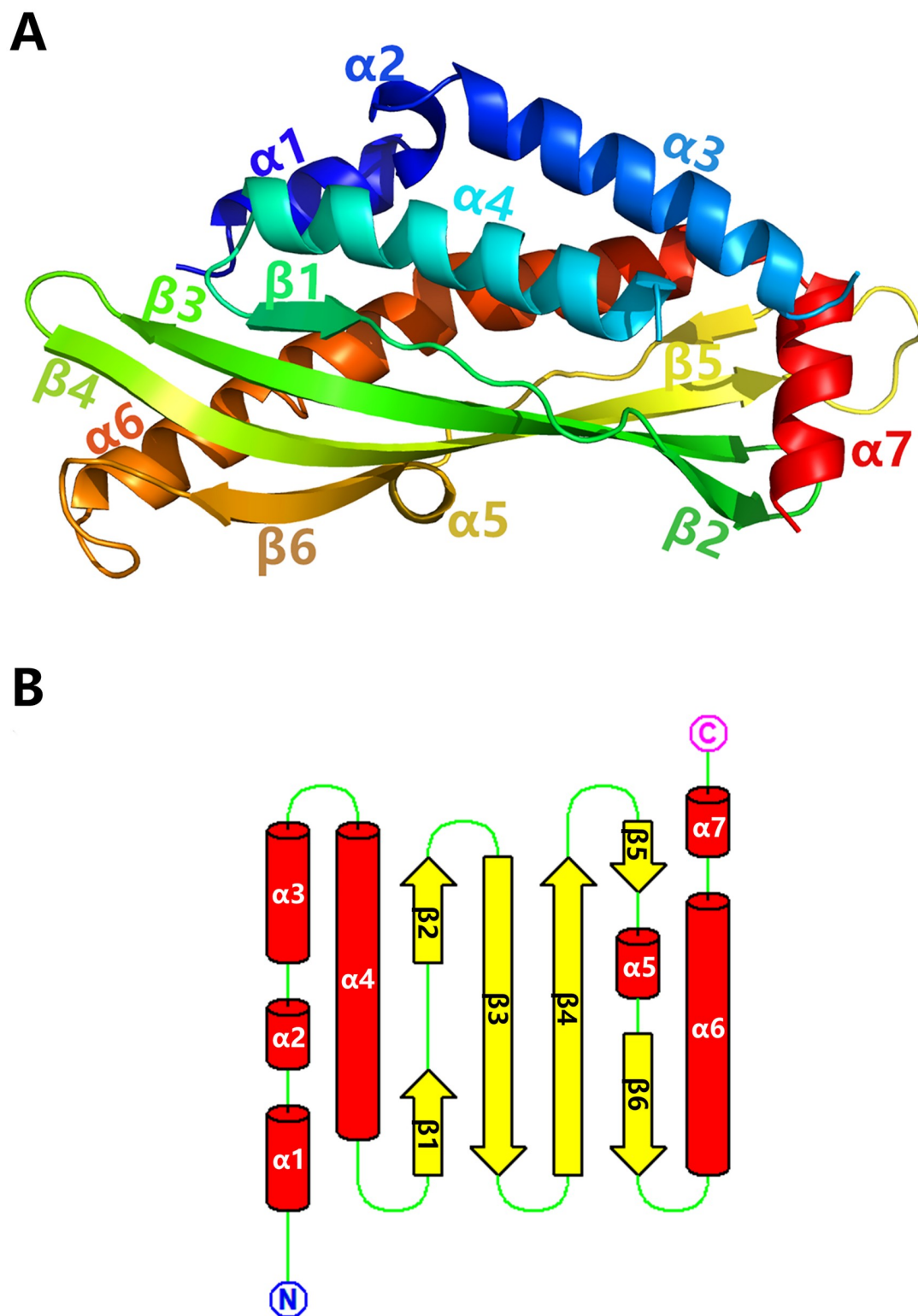


**Fig 1. Structure of BSP30b.** (A) the tertiary structure of apo-BSP30b, coloured in rainbow mode ranging from blue (N terminus) to red (C terminus). (B) topology diagram of BSP30b. All seven  $\alpha$  helices are represented by red cylinders; six  $\beta$  strands by yellow arrows; green lines represent the loops and turns.

<https://doi.org/10.1371/journal.pone.0206709.g001>

joins the long curved helix  $\alpha_6$  and the loop region between helix  $\alpha_5$  and strand  $\beta_5$ . This disulfide bond has been proposed to contribute to the stability of the overall structure [28].

### Structural comparison

The BSP30b structure was compared with other structures in the PDB using PDBeFold. From the structural alignment, two proteins are related: SPLUNC1 from human (Fig 2A, PDB code 4KGG) with a Z score of 4.8 and a root mean squared deviation (RMSD) for C $\alpha$  atoms of 3.2 Å (total of 144 residues aligned); and BPIFA1 from mouse with a Z score of 5.4 and RMSD for C $\alpha$  positions of 3.4 Å (total of 151 residues aligned). All three proteins have the archetypal tubular structure with the conserved hydrophobic channel and the conserved disulfide bond (Fig 2A and 2B) at the same position.

As SPLUNC1 and BPIFA1 are closely related, we take the comparison between BSP30b and SPLUNC1 as an example. There are two obvious disparities between these two structures. The first difference results from the presence of a second disulfide bond in BSP30b (Fig 2B). This second disulfide bond, formed between Cys72 and Cys229, connects the flexible loop just after helix  $\alpha_3$  to the C-terminal helix  $\alpha_7$  (Fig 2B). Intriguingly the electron density for the disulphide bond is only clear in one molecule of the asymmetric unit and missing in the other. This may indicate that this disulfide bond is partially reduced under the crystallisation conditions.

The second obvious difference between the two structures is that both the N-terminus and C-terminus of SPLUNC1 are located at the same end of its long axis, whilst the termini of BSP30b are located at opposite ends of the long axis (Fig 2C). That is to say that the first three N-terminal  $\alpha$  helices in BSP30b have no structural equivalent in SPLUNC1. This structural difference influences the geometry of the opening of the ligand binding cavity. For BSP30b, the entrance to the ligand binding site is adjacent to the C-terminal helix  $\alpha_7$  and is potentially

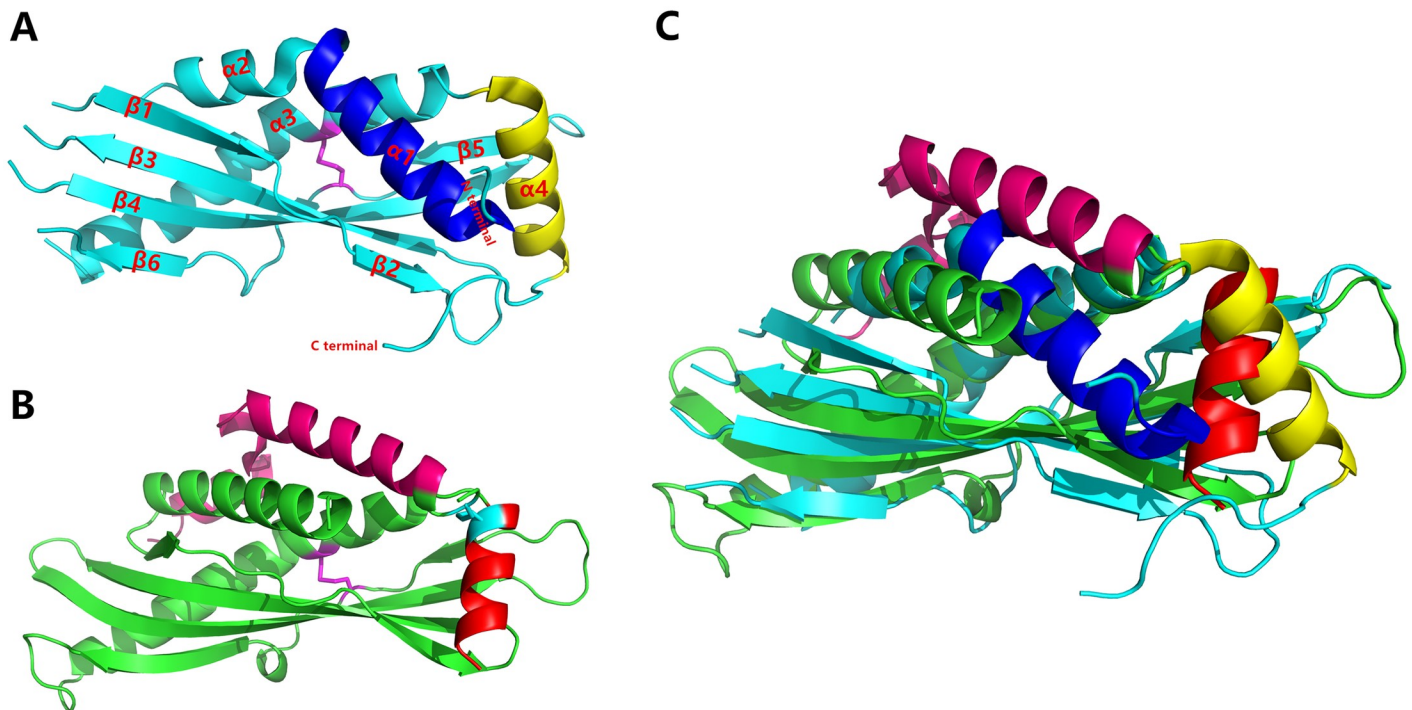


**Fig 2. Structural comparison between BSP30b with hSPLUNC1.** (A) the structure of hSPLUNC1, with its disulfide bond shown in magenta. (B) the structure of BSP30b. The conserved disulfide bond is shown in magenta and the second disulfide bond is shown in cyan. (C) structural alignment of BSP30b to hSPLUNC1. BSP30b is shown in cyan and hSPLUNC1 is shown in green. Their structural differences are marked with different colours as per A and B.

<https://doi.org/10.1371/journal.pone.0206709.g002>

influenced by the flexible loop between helices  $\alpha 3$  and  $\alpha 4$ . Whereas for SPLUNC1, the entrance to the cavity is dominated by the long N-terminal helix (in blue in Fig 2C). Because of the geometric rearrangement of the hydrophobic channel opening, BSP30b has a much larger internal cavity compared to SPLUNC1 as calculated using the CASTp 3.0 online server [27]. The volume of the cavity of SPLUNC1 is  $37.7 \text{ \AA}^3$ , whilst the cavity of BSP30b has a volume of  $90.2 \text{ \AA}^3$ . The enlarged internal cavity of BSP30b could make it more accessible by its potential ligands.

The structure of BSP30b was also compared with the TULIP proteins whose structures have been deposited in the PDB. A sequence alignment of the corresponding PFam family (PF01273) [29] shows that the two cysteine residues that constitute the conserved disulphide bond are the only well conserved feature of the multiple sequence alignment. Hence the conservation of structure is the defining feature for this family. Generally, the secondary structures constituting the tubular channel are well conserved among all of the proteins. It is also clear that the C-terminal domains of BPI (1ewf), LBP (4m4d), and CETP (2obd) are well aligned but are different from E-syt 2 (4p42). This is because the C-terminal domain of E-syt 2 interacts with lipid bilayers, rather than lipid binding/transportation [30].

### Structure of BSP30b with oleic acid in the hydrophobic tunnel

Since the primary lipid sources for cattle are linolenic acid, linoleic acid, and oleic acid from pasture grass, we speculated that those fatty acids may be substrates for BSP30b. Thus, the binding of these three fatty acids were examined by co-crystallisation separately. Several structures were determined from crystals grown from mixtures of BSP30b and various fatty acids and fatty acid derivatives (e.g. methyl oleic ester). The only structure that revealed elongated stretches of electron density within the hydrophobic tunnel was the complex between BSP30b and oleic acid. The hydrophobic end of oleic acid is buried in the tunnel and its carboxyl group stretches out from the tunnel's opening, forming hydrogen bonds with the carboxyl group of ASP112 and the carbonyl group of ILE113 (Fig 3A and 3B). We suggest that the hydrophobic tail of oleic acid first "glides" into the internal cavity, driven by multiple hydrophobic interactions, while its carboxyl group stretches out and is stabilised by forming hydrogen bonds with the proximate amino acids. A similar hypothesis has been proposed for *Epiphyas postvittana* Takeout 1 protein [31], where both fatty acid ligands (including the head groups) "slide down" into the hydrophobic tunnel.

We also observe that the overall structure of BSP30b and its internal cavity remain almost completely unchanged upon binding of the lipid ligand, suggesting that the internal cavity of BSP30b also forms a rigid scaffold for its lipid ligands. Only the helix  $\alpha 3$  moves slightly away.

It is noteworthy that the electron density of oleic acid is clear in one molecule of the asymmetric unit but incomplete for oleic acid in the other molecule (Fig 3D). This may suggest that oleic acid is not the preferred ligand of BSP30b. An mFo-DFc polder (OMIT) map contoured at  $3 \sigma$  (Fig 3D) also confirmed this finding. For both oleic acid molecules in the asymmetric unit, CCm1-m3 values are larger than CCm1-m2 and CCm2-m3 values, suggesting that both of the hydrophobic channels contain oleic acid and not bulk solvent (Table 2). One of these sites is occupied to a greater extent than the other and a refinement of the occupancy for the binding site of the dominant ligand showed 80% occupancy for this molecule.

### GFP\_BSP30b is an emulsifier with olive oil

Twenty minutes after mixing GFP\_BSP30b with olive oil, two layers were formed. The top layer was thin and cloudy whereas the bottom layer was slightly cloudy. When the bottom layer was viewed under blue light by fluorescent microscopy, an emulsion was seen with GFP\_BSP30b decorating the surface of each small droplet, indicated by its green fluorescence

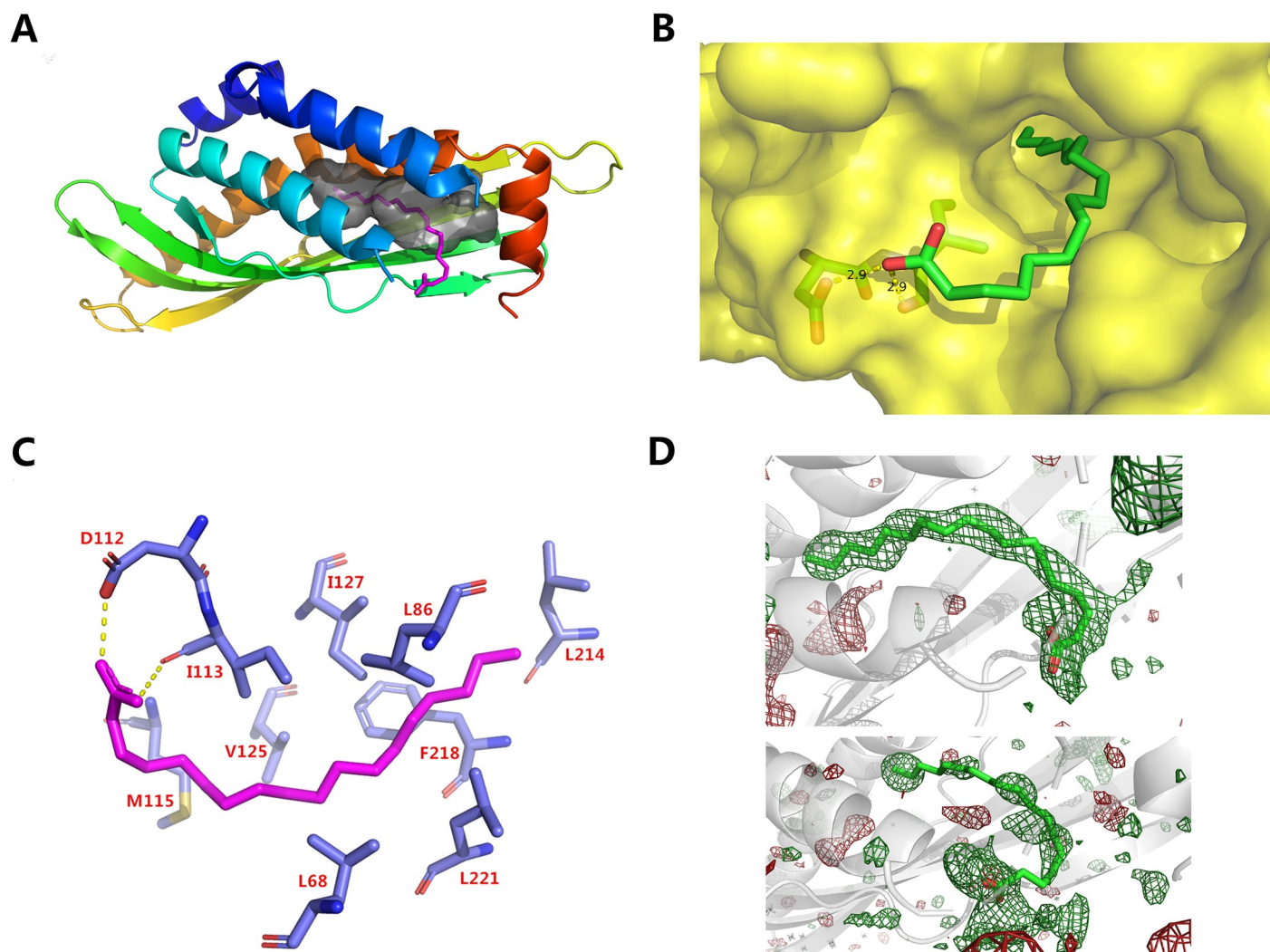


**Fig 3. Structure of BSP30b with oleic acid.** (A) Oleic acid is coloured in magenta and occupies the internal cavity, shown in grey. (B) surface representation of the binding pocket with oleic acid. Hydrogen bonds between the carboxyl group of oleic acid and carboxyl group of ASP112, and backbone carbonyl group of ILE113 are shown as yellow dashed lines. (C) Residues interacting with oleic acid within 4 Å. Oleic acid is shown in pink. (D) polder (OMIT) map for both oleic acids in the ASU. The positive and negative  $mF_o - DFC$  difference density contoured at  $3\sigma$  is displayed in green and red, respectively. All structural illustrations were prepared with PyMOL.

<https://doi.org/10.1371/journal.pone.0206709.g003>

(Fig 4A). The top thin layer also has a similar composition but the micelles seen are larger and more compact. In decorating the surface of oil droplets, BSP30b may stabilise the small oil droplets in solution and thus, act as an emulsifier. This observation is consistent with the original finding by Wheeler and colleagues [8] that BSP proteins are protective for bloat in cattle.

**Table 2. Local correlation coefficients (CC) and CC peak values for the three polder (OMIT) maps: m1, m2 and m3.**

	Oleic acid in the first molecule of ASU		Oleic acid in the second molecule of ASU	
	CC	CC <sub>peak</sub>	CC	CC <sub>peak</sub>
m1-m2	0.6280	0.6532	0.6059	0.6350
m1-m3	0.8639	0.8733	0.7601	0.7929
m2-m3	0.6137	0.6255	0.6126	0.6185

<https://doi.org/10.1371/journal.pone.0206709.t002>

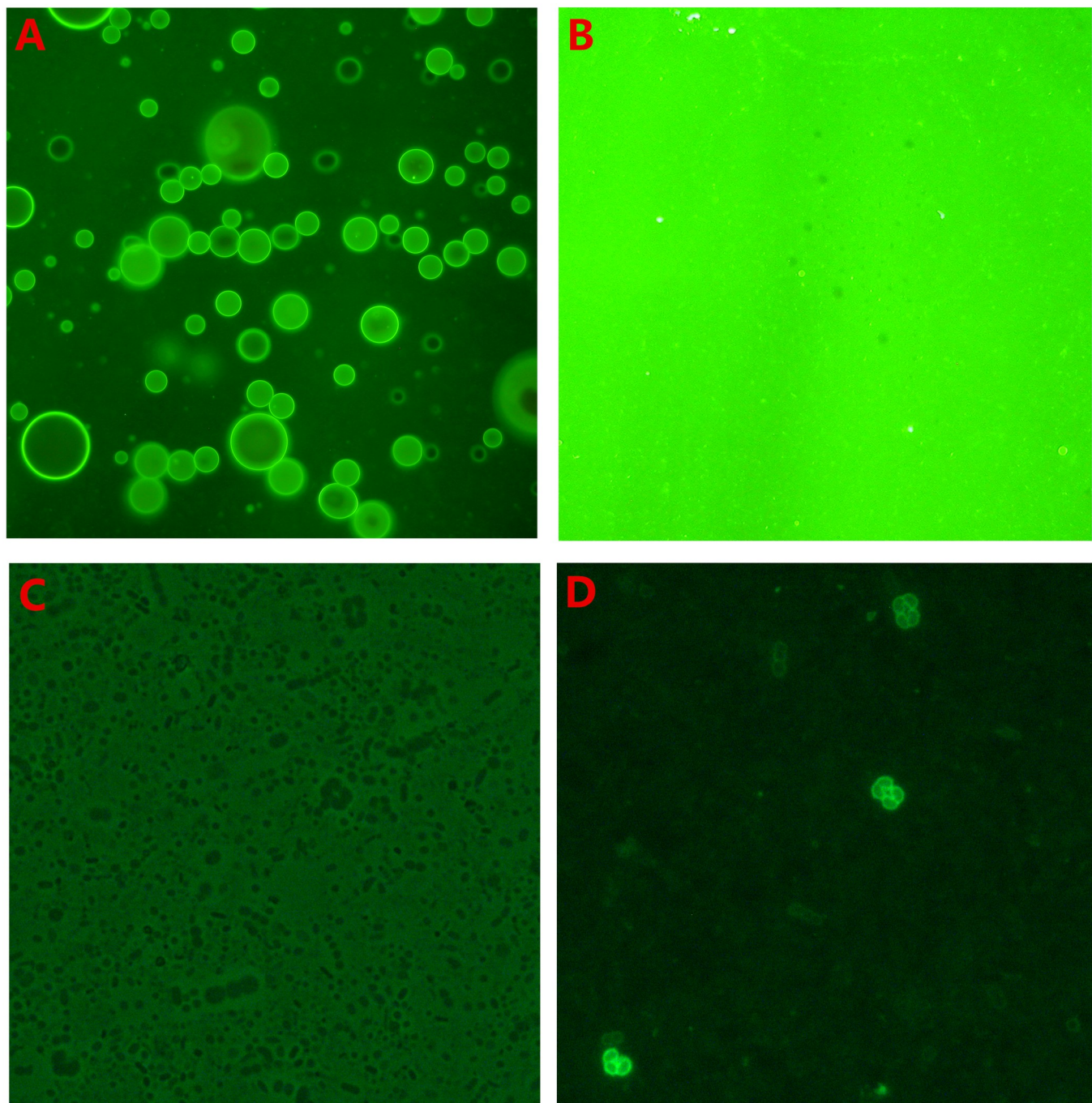


**Fig 4. Fluorescent microscopy of GFP\_BSP30b coating olive oil/rumen bacteria.** (A) emulsion formed after mixing of GFP\_BSP30b with olive oil. BSP30b decorates the surface of each droplet, indicated by green fluorescence from its fused GFP under UV illumination. (B) control experiment using GFP alone mixed with olive oil confirmed no emulsification or decoration by GFP. (C) and (D) comparison of the view of rumen bacteria mixed with GFP\_BSP30b under bright field (C) and UV illumination (D).

<https://doi.org/10.1371/journal.pone.0206709.g004>

### GFP\_BSP30b binding to the surface of specific rumen bacterial strains

A surprising preliminary result is the observation that the mixture of GFP\_BSP30b with ruminant bacteria observed under UV illumination shows that BSP30b binds to just a small

number of rumen bacterial cells. BSP30b showed strong binding to a short and curved rod-like bacterial strain, which is clustered as triad or tetrad (Fig 4D). Whereas BSP30b does not bind to the majority of bacteria in the field of view. We observed that BSP30b can also bind to a few cocci-shaped cells but with weaker fluorescence suggesting a weaker equilibrium constant for binding to these bacteria. We suggest that the binding specificity of BSP30b to certain bacterial surface lipids may result in its binding selectivity to a small subset of rumen bacterial strains and characterising these strains is the subject of ongoing work in our laboratory.

## Discussion

Currently, the bovine PLUNC family has 13 members including BSP30a-d that have likely arisen through recent gene duplication [13]. Although BSP30 gene expression has been well-studied at both the mRNA level and the protein level, their biological functions are poorly understood. The lack of structural information or knowledge about the lipid substrates for the cattle PLUNC family members impedes our understanding of their function.

Here, we report the first crystal structures of BSP30b at 2.0 Å resolution. We have shown that the TULIP superfamily architecture is maintained with the characteristic internal hydrophobic channel formed by an  $\alpha/\beta$  wrap fold. Structural comparison to the closest related structures in the PDB (human SPLUNC1 and mouse BPIFA1) has revealed both conserved and unique features that might be important for function. The unique disulfide bond present in BSP30b but not in other PLUNC proteins may play a role in ligand binding as it links the C-terminal helix with the protein body and the C-terminal helix lies adjacent to the ligand tunnel. Further evidence for this includes the fact that a similar disulfide bond is also found in the structure of Takeout 1 of *Epiphyas postvittana* and JHBP of silkworm, which are also members of the TULIP superfamily. Their disulfide bonds are reported to have a critical role in ligand binding rather than maintaining the stability of the bulk structure [31, 32].

Compared to human SPLUNC1, the internal cavity opening of BSP30b is much larger. This results from the reorganisation of the termini of the protein such that the C-terminus of BSP30b lies at the entrance to the ligand binding tunnel. For SPLUNC1, its N-terminal helix  $\alpha 1$  and C-terminal helix  $\alpha 4$ , together with helix  $\alpha 3$ , form the predicted ligand binding site of SPLUNC1 and it is hypothesized that helix  $\alpha 1$  moves away to “open-up” the binding site upon lipid binding [28]. From our BSP30b-oleic acid structure, it is obvious that, unlike the changes proposed for SPLUNC1, no major conformational change is needed for lipid binding. Only helix  $\alpha 3$  has moved away slightly from the core structure upon oleic acid binding. Ligand binding may be related to oxidation/reduction of the disulphide bond that links the C-terminal helix in a similar manner to the takeout proteins.

This is also the first time that a PLUNC family protein has been crystallized with its ligand, although the electron density for the ligand suggests 80% occupancy. We have tried to crystallize BSP30b with linolenic acid and linoleic acid, but in the structural data no electron density was found for either of these fatty acids. Linolenic acid and linoleic acid have more rigid structures compared to oleic acid as they have three and two double bonds on their carbon backbones, respectively. In contrast, oleic acid has only one double bond, which gives it more flexibility to occupy the relatively narrow hydrophobic channel.

Proteins in the PLUNC family have been shown to have potent surfactant properties at water/liquid interfaces [33, 34]. We demonstrated that BSP30b also behaves like an emulsifier, dispersing olive oil into small droplets in aqueous solution. This may be relevant to the original observation that high BSP30 expressing animals had lower susceptibility to bloat (which is caused by uncontrolled foaming in the rumen).

We find it intriguing that BSP30b only binds to a small subset of bacterial cells within the rumen. “Bacteria coating” by proteins from the PLUNC group has been reported before [35, 36]. Murine PSP was shown to bind to specific membrane proteins of *E. coli*, *S. mutans*, *A. actinomycetemcomitans*, and *L. monocytogenes*, and the interactions are dependent on the presence of  $Zn^{2+}$ . We suggest that BSP30b binds to specific lipids on the bacterial surface based on the crystal structure and oleic acid binding. The “bacterial cell coating” by human SPLUNC1 of *P. aeruginosa*-pMF230 has been investigated using confocal microscopy, and the protein is proposed to display a bacteriostatic property preventing bacterial growth. Other studies also report that anti-biofilm properties of human SPLUNC1 may due to its role as a surfactant [37]. In light of our structure and functional experiments with BSP30b we suggest that this abundant salivary protein could have important roles in the rumen via its binding specificity to certain ruminal bacteria species and identifying the specific bacterial species and the nature of the interaction is the subject of ongoing work.

## Acknowledgments

We would like to thank DairyNZ (Hamilton, New Zealand) for their support on this project. This research was undertaken in part using the MX2 beamline at the Australian Synchrotron, part of ANSTO, and made use of the Australian Cancer Research Foundation (ACRF) detector.

## Author Contributions

**Conceptualization:** Tom T. Wheeler, Vickery L. Arcus.

**Formal analysis:** Vickery L. Arcus.

**Methodology:** Heng Zhang, Judith Burrows, Graeme L. Card, Graeme Attwood, Tom T. Wheeler.

**Resources:** Judith Burrows.

**Supervision:** Graeme Attwood, Vickery L. Arcus.

**Writing – original draft:** Heng Zhang.

**Writing – review & editing:** Heng Zhang, Graeme L. Card, Graeme Attwood, Tom T. Wheeler, Vickery L. Arcus.

## References

1. Canny G, Levy O. Bactericidal/permeability-increasing protein (BPI) and BPI homologs at mucosal sites. *Trends in immunology*. 2008; 29(11):541–7. <https://doi.org/10.1016/j.it.2008.07.012> PMID: 18838299.
2. LeClair EE. Four reasons to consider a novel class of innate immune molecules in the oral epithelium. *Journal of dental research*. 2003; 82(12):944–50. <https://doi.org/10.1177/154405910308201202> PMID: 14630892.
3. Ghafouri B, Stahlbom B, Tagesson C, Lindahl M. Newly identified proteins in human nasal lavage fluid from non-smokers and smokers using two-dimensional gel electrophoresis and peptide mass fingerprinting. *Proteomics*. 2002; 2(1):112–20. PMID: 11788998.
4. Ghafouri B, Kihlstrom E, Tagesson C, Lindahl M. PLUNC in human nasal lavage fluid: multiple isoforms that bind to lipopolysaccharide. *Biochimica et biophysica acta*. 2004; 1699(1–2):57–63. <https://doi.org/10.1016/j.bbapap.2004.01.001> PMID: 15158712.
5. Bartlett JA, Hicks BJ, Schlomann JM, Ramachandran S, Nauseef WM, McCray PB Jr. PLUNC is a secreted product of neutrophil granules. *Journal of leukocyte biology*. 2008; 83(5):1201–6. <https://doi.org/10.1189/jlb.0507302> PMID: 18245229.

6. Kopec KO, Alva V, Lupas AN. Bioinformatics of the TULIP domain superfamily. *Biochemical Society transactions*. 2011; 39(4):1033–8. <https://doi.org/10.1042/BST0391033> PMID: 21787343.
7. Alva V, Lupas AN. The TULIP superfamily of eukaryotic lipid-binding proteins as a mediator of lipid sensing and transport. *Biochimica et biophysica acta*. 2016; 1861(8 Pt B):913–23. <https://doi.org/10.1016/j.bbali.2016.01.016> PMID: 26825693.
8. Rajan GH, Morris CA, Carruthers VR, Wilkins RJ, Wheeler TT. The relative abundance of a salivary protein, bSP30, is correlated with susceptibility to bloat in cattle herds selected for high or low bloat susceptibility. *Anim Genet*. 1996; 27(6):407–14. PMID: 9022155
9. Clarke RT, Reid CS. Foamy bloat of cattle. A review. *Journal of dairy science*. 1974; 57(7):753–85. [https://doi.org/10.3168/jds.S0022-0302\(74\)84964-7](https://doi.org/10.3168/jds.S0022-0302(74)84964-7) PMID: 4601637.
10. Bingle CD, Seal RL, Craven CJ. Systematic nomenclature for the PLUNC/PSP/BSP30/SMGB proteins as a subfamily of the BPI fold-containing superfamily. *Biochemical Society transactions*. 2011; 39(4):977–83. <https://doi.org/10.1042/BST0390977> PMID: 21787333.
11. Wheeler TT, Haigh BJ, McCracken JY, Wilkins RJ, Morris CA, Grigor MR. The BSP30 salivary proteins from cattle, LUNX/PLUNC and von Ebner's minor salivary gland protein are members of the PSP/LBP superfamily of proteins. *Biochimica et biophysica acta*. 2002; 1579(2–3):92–100. PMID: 12427544.
12. Wheeler TT, Hood KA, Maqbool NJ, McEwan JC, Bingle CD, Zhao SY. Expansion of the bactericidal/permeability increasing-like (BPI-like) protein locus in cattle. *Bmc Genomics*. 2007; 8. Artn 75 <https://doi.org/10.1186/1471-2164-8-75> PMID: 17362520
13. Haigh B, Hood K, Broadhurst M, Medele S, Callaghan M, Smolenski G, et al. The bovine salivary proteins BSP30a and BSP30b are independently expressed BPI-like proteins with anti-*Pseudomonas* activity. *Mol Immunol*. 2008; 45(7):1944–51. <https://doi.org/10.1016/j.molimm.2007.10.032> PMID: 18055015
14. Wheeler TT, Hood K, Oden K, McCracken J, Morris CA. Bovine parotid secretory protein: structure, expression and relatedness to other BPI (bactericidal/permeability-increasing protein)-like proteins. *Biochemical Society transactions*. 2003; 31(Pt 4):781–4.
15. Wheeler TT, Haigh BJ, Broadhurst MK, Hood KA, Maqbool NJ. The BPI-like/PLUNC family proteins in cattle. *Biochemical Society transactions*. 2011; 39:1006–11. <https://doi.org/10.1042/BST0391006> PMID: 21787338
16. Leslie AGW, Powell HR. Processing diffraction data with MOSFLM. *Nato Sci Ser Li-Math*. 2007; 245:41–+.
17. Evans PR, Murshudov GN. How good are my data and what is the resolution? *Acta Crystallogr D*. 2013; 69:1204–14. <https://doi.org/10.1107/S0907444913000061> PMID: 23793146
18. Collaborative Computational Project N. The CCP4 suite: programs for protein crystallography. *Acta crystallographica Section D, Biological crystallography*. 1994; 50(Pt 5):760–3. <https://doi.org/10.1107/S0907444994003112> PMID: 15299374.
19. Terwilliger TC, Adams PD, Read RJ, McCoy AJ, Moriarty NW, Grosse-Kunstleve RW, et al. Decision-making in structure solution using Bayesian estimates of map quality: the PHENIX AutoSol wizard. *Acta Crystallogr D*. 2009; 65:582–601. <https://doi.org/10.1107/S0907444909012098> PMID: 19465773
20. Terwilliger TC, Grosse-Kunstleve RW, Afonine PV, Moriarty NW, Zwart PH, Hung LW, et al. Iterative model building, structure refinement and density modification with the PHENIX AutoBuild wizard. *Acta Crystallogr D*. 2008; 64:61–9. <https://doi.org/10.1107/S090744490705024X> PMID: 18094468
21. Adams PD, Afonine PV, Bunkoczi G, Chen VB, Echols N, Headd JJ, et al. The Phenix software for automated determination of macromolecular structures. *Methods*. 2011; 55(1):94–106. <https://doi.org/10.1016/j.ymeth.2011.07.005> PMID: 21821126
22. Afonine PV, Grosse-Kunstleve RW, Adams PD. A robust bulk-solvent correction and anisotropic scaling procedure. *Acta Crystallogr D*. 2005; 61:850–5. <https://doi.org/10.1107/S0907444905007894> PMID: 15983406
23. Emsley P, Cowtan K. Coot: model-building tools for molecular graphics. *Acta Crystallogr D*. 2004; 60:2126–32. <https://doi.org/10.1107/S0907444904019158> PMID: 15572765
24. McPhillips TM, McPhillips SE, Chiu HJ, Cohen AE, Deacon AM, Ellis PJ, et al. Blu-Ice and the Distributed Control System: software for data acquisition and instrument control at macromolecular crystallography beamlines. *Journal of synchrotron radiation*. 2002; 9(Pt 6):401–6. PMID: 12409628.
25. McCoy AJ, Grosse-Kunstleve RW, Adams PD, Winn MD, Storoni LC, Read RJ. Phaser crystallographic software. *J Appl Crystallogr*. 2007; 40:658–74. <https://doi.org/10.1107/S0021889807021206> PMID: 19461840
26. Liebschner D, Afonine PV, Moriarty NW, Poon BK, Sobolev OV, Terwilliger TC, et al. Polder maps: improving OMIT maps by excluding bulk solvent. *Acta crystallographica Section D, Structural biology*. 2017; 73(Pt 2):148–57. <https://doi.org/10.1107/S2059798316018210> PMID: 28177311.

27. Tian W, Chen C, Lei X, Zhao J, Liang J. CASTp 3.0: computed atlas of surface topography of proteins. *Nucleic acids research*. 2018; 46(W1):W363–W7. <https://doi.org/10.1093/nar/gky473> PMID: 29860391.
28. Ning FK, Wang C, Berry KZ, Kandasamy P, Liu HL, Murphy RC, et al. Structural characterization of the pulmonary innate immune protein SPLUNC1 and identification of lipid ligands. *Faseb J*. 2014; 28(12):5349–60. <https://doi.org/10.1096/fj.14-259291> PMID: 25223608
29. Finn RD, Coghill P, Eberhardt RY, Eddy SR, Mistry J, Mitchell AL, et al. The Pfam protein families database: towards a more sustainable future. *Nucleic acids research*. 2016; 44(D1):D279–85. <https://doi.org/10.1093/nar/gkv1344> PMID: 26673716.
30. Schauder CM, Wu X, Saheki Y, Narayanaswamy P, Torta F, Wenk MR, et al. Structure of a lipid-bound extended synaptotagmin indicates a role in lipid transfer. *Nature*. 2014; 510(7506):552–5. <https://doi.org/10.1038/nature13269> PMID: 24847877.
31. Hamiaux C, Basten L, Greenwood DR, Baker EN, Newcomb RD. Ligand promiscuity within the internal cavity of Epiphyas postvittana Takeout 1 protein. *Journal of structural biology*. 2013; 182(3):259–63. <https://doi.org/10.1016/j.jsb.2013.03.013> PMID: 23563188.
32. Suzuki R, Fujimoto Z, Shiotsuki T, Tsuchiya W, Momma M, Tase A, et al. Structural mechanism of JH delivery in hemolymph by JHBP of silkworm, *Bombyx mori*. *Scientific reports*. 2011; 1:133. <https://doi.org/10.1038/srep00133> PMID: 22355650.
33. Bartlett JA, Gakhar L, Penterman J, Singh PK, Mallampalli RK, Porter E, et al. PLUNC: a multifunctional surfactant of the airways. *Biochemical Society transactions*. 2011; 39(4):1012–6. <https://doi.org/10.1042/BST0391012> PMID: 21787339.
34. McDonald RE, Fleming RI, Beeley JG, Bovell DL, Lu JR, Zhao X, et al. Latherin: a surfactant protein of horse sweat and saliva. *Plos One*. 2009; 4(5):e5726. <https://doi.org/10.1371/journal.pone.0005726> PMID: 19478940.
35. Robinson CP, Bounous DI, Alford CE, Nguyen KH, Nanni JM, Peck AB, et al. PSP expression in murine lacrimal glands and function as a bacteria binding protein in exocrine secretions. *The American journal of physiology*. 1997; 272(4 Pt 1):G863–71. <https://doi.org/10.1152/ajpgi.1997.272.4.G863> PMID: 9142919.
36. Sayeed S, Nistico L, St Croix C, Di YP. Multifunctional role of human SPLUNC1 in *Pseudomonas aeruginosa* infection. *Infect Immun*. 2013; 81(1):285–91. <https://doi.org/10.1128/IAI.00500-12> PMID: 23132494.
37. Gakhar L, Bartlett JA, Penterman J, Mizrahi D, Singh PK, Mallampalli RK, et al. PLUNC is a novel airway surfactant protein with anti-biofilm activity. *Plos One*. 2010; 5(2):e9098. <https://doi.org/10.1371/journal.pone.0009098> PMID: 20161732.